J Mar Sci Technol (2015) 20:37–52
DOI 10.1007/s00773-014-0293-y

REVIEW ARTICLE

Introduction of MMG standard method for ship maneuvering predictions

H. Yasukawa · Y. Yoshimura

Received: 6 February 2014 / Accepted: 19 October 2014 / Published online: 8 November 2014

Abstract A lot of simulation methods based on Maneuvering Modeling Group (MMG) model for ship maneuvering have been presented. Many simulation methods sometimes harm the adaptability of hydrodynamic force data for the maneuvering simulations since one method may be not applicable to other method in general. To avoid this, basic part of the method should be common. Under such a background, research committee on "standardization of mathematical model for ship maneuvering predictions" was organized by the Japan Society of Naval Architects and Ocean Engineers and proposed a prototype of maneuvering prediction method for ships, called "MMG standard method". In this article, the MMG standard method is introduced. The MMG standard method is composed of 4 elements; maneuvering simulation model, procedure of the required captive model tests to capture the hydrodynamic force characteristics, analysis method for determining the hydrodynamic force coefficients for maneuvering simulations, and prediction method for maneuvering motions of a ship in fullscale. KVLCC2 tanker is selected as a sample ship and the captive mode test results are presented with a process of the data analysis. Using the hydrodynamic force coefficients presented, maneuvering simulations are carried out for KVLCC2 model and the fullscale ship for validation of the method. The present method can roughly capture the maneuvering motions and is useful for the maneuvering predictions in fullscale.

H. Yasukawa (✉)
Graduate School of Engineering, Hiroshima University, Higashi-hiroshima, Japan
e-mail: yasukawa@naoe.hiroshima-u.ac.jp

Y. Yoshimura
Graduate School of Fisheries Sciences, Hokkaido University, Hakodate, Japan

Keywords MMG standard method · MMG model · Maneuvering prediction · KVLCC2 · Captive model tests

List of symbols

A_D	Advance
A_R	Profile area of movable part of mariner rudder
a_H	Rudder force increase factor
B	Ship breadth
B_R	Averaged rudder chord length
C_b	Block coefficient
C_1, C_2	Experimental constants representing wake characteristic in maneuvering
D_P	Propeller diameter
D_T	Tactical diameter
d	Ship draft
F_N	Rudder normal force
F_n	Froude number based on ship length
F_x, F_y	Surge force and lateral force acting on ship
f_α	Rudder lift gradient coefficient
H_R	Rudder span length
I_{zG}	Moment of inertia of ship around center of gravity
J_P	Propeller advanced ratio
J_z	Added moment of inertia
K_T	Propeller thrust open water characteristic
k_2, k_1, k_0	Coefficients representing K_T
L_{pp}	Ship length between perpendiculars
ℓ_R	Effective longitudinal coordinate of rudder position in formula of β_R
M_z	Yaw moment acting on ship around center of gravity

m	Ship's mass
m_x, m_y	Added masses of x axis direction and y axis direction, respectively
n_{P}	Propeller revolution
$o-xyz$	Ship fixed coordinate system taking the origin at midship
$o_0-x_0y_0z_0$	Space fixed coordinate system
R'_0	Ship resistance coefficient in straight moving
r	Yaw rate
T	Propeller thrust
t	Time
t_{P}	Thrust deduction factor
t_{R}	Steering resistance deduction factor
U	Resultant speed ($=\sqrt{u^2+v_m^2}$)
U_0	Approach ship speed (given speed)
U_R	Resultant inflow velocity to rudder
u, v	Surge velocity, lateral velocity at center of gravity, respectively
u_R, v_R	Longitudinal and lateral inflow velocity components to rudder, respectively
v_m	Lateral velocity at midship
w_{P}	Wake coefficient at propeller position in maneuvering motions
w_{P0}	Wake coefficient at propeller position in straight moving
w_{R}	Wake coefficient at rudder position
X, Y, N_m	Surge force, lateral force, yaw moment around midship except added mass components
X_H, Y_H, N_H	Surge force, lateral force, yaw moment around midship acting on ship hull except added mass components X_{P} Surge force due to propeller
X_R, Y_R, N_R	Surge force, lateral force, yaw moment around midship by steering
X_{mes}, Y_{mes}, N_{mes}	Surge force, lateral force, yaw moment around midship measured in CMT
x_G	Longitudinal coordinate of center of gravity of ship
x_{H}	Longitudinal coordinate of acting point of the additional lateral force component induced by steering
x_{P}	Longitudinal coordinate of propeller position
x_{R}	Longitudinal coordinate of rudder position ($=-0.5L_{pp}$)
Y'_v, N'_v	Linear hydrodynamic derivatives with respect to lateral velocity
$Y'_{\mathrm{R}}, N'_{\mathrm{R}}$	Linear hydrodynamic derivatives with respect to yaw rate
α_R	Effective inflow angle to rudder
β	Hull drift angle at midship
β_{P}	Geometrical inflow angle to propeller in maneuvering motions
β_{R0}	Geometrical inflow angle to rudder in maneuvering motions
β_{R}	Effective inflow angle to rudder in maneuvering motions
γ_R	Flow straightening coefficient
δ	Rudder angle
δ_{FN0}	Rudder angle where rudder normal force becomes zero
η	Ratio of propeller diameter to rudder span ($=D_{\mathrm{P}}/H_{\mathrm{R}}$)
Λ	Rudder aspect ratio
κ	An experimental constant for expressing u_{R}
∇	Displacement volume of ship
ψ	Ship heading
ρ	Water density
ε	Ratio of wake fraction at propeller and rudder positions ($=(1-w_{\mathrm{R}})/(1-w_{\mathrm{P}})$)

1 Introduction

MMG model is one of the solutions for ship maneuvering motion simulations developed in Japan. The model was proposed by a research group called Maneuvering Modeling Group (MMG) in Japanese Towing Tank Conference (JTTC), and the outline was reported in the Bulletin of Society of Naval Architects of Japan [1] in 1977. In the report, the concept for maneuvering simulations was mainly described, but concrete simulation model was not described in detail. According to MMG model concept, afterward, concrete methods including expression of hydrodynamic forces acting on ships were presented by Ogawa and Kasai [2], Matsumoto and Suemitsu [3], Inoue et al. [4] and so on. Nowadays, a lot of simulation methods based on MMG model are existing.

Many simulation methods sometimes harm the adaptability of hydrodynamic force data for the maneuvering simulations since one method may be not applicable to other method in general. To avoid this, basic part of the method should be common. The test procedure and the data analysis to determine the hydrodynamic force coefficients for the simulations should be also common since those often involve the quantitative value of the hydrodynamic coefficients.

Under such a background, the research committee on "standardization of mathematical model for ship

maneuvering predictions" organized by the Japan Society of Naval Architects and Ocean Engineers has checked the details of existing MMG models such as the coordinate system, the motion equations, the hull and rudder hydrodynamic force models etc., in view of accuracy, simplicity, physical/theoretical background and adoptability to the captive model tests for capturing the hydrodynamic force characteristics. As the conclusion, a prototype of maneuvering simulation method for ships called "MMG standard method", has been proposed [5].

This article introduces the MMG standard method which is composed of 4 elements:

- maneuvering simulation model,
- procedure of the required captive model tests to capture the hydrodynamic force characteristics,
- analysis method for determining the hydrodynamic force coefficients for maneuvering simulations, and
- prediction method for maneuvering motions of a ship in fullscale.

The basic simulation model described here is a combination of the existing models for expressing the hydrodynamic force characteristics with respect to ship hull, propeller, rudder, and their interaction components. The physical meaning of the models is described in detail for the better understanding. KVLCC2 tanker is selected as a sample ship and the captive mode test results [6, 7] are presented with a process of the data analysis. It may be a special feature of this article that the test procedure and the data analysis to determine the hydrodynamic force coefficients are presented in detail. Using the hydrodynamic force coefficients determined, maneuvering simulations are carried out for KVLCC2 model [8] and the fullscale ship for validation of the method.

2 Maneuvering simulation model

First, the motion equations to express the maneuvering motions for a ship with single propeller and single rudder, and the simulation model of hydrodynamic forces acting on the ship are described.

In this article, prime $'$ putting to the symbol means non-dimensionalized value. Force and moment are non-dimensionalized by $(1/2)\rho L_{pp} d U^2$ and $(1/2)\rho L_{pp}^2 d U^2$, respectively. In addition, mass and moment of inertia are non-dimensionalized by $(1/2)\rho L_{pp}^2 d$ and $(1/2)\rho L_{pp}^4 d$, respectively. Velocity component is non-dimensionalized by U and length component is by L_{pp}.

2.1 Assumptions and coordinate systems

The following assumptions are employed:

- Ship is a rigid body.
- Hydrodynamic forces acting on the ship are treated quasi-steadily.
- Lateral velocity component is small compared with longitudinal velocity component.
- Ship speed is not fast that wave-making effect can be neglected.
- Metacentric height $\overline{GM}$ is sufficiently large, and the roll coupling effect on maneuvering is negligible.

Figure 1 shows the coordinate systems used in the present article: the space-fixed coordinate system o_0–$x_0y_0z_0$, where x_0–y_0 plane coincides with the still water surface and z_0 axis points vertically downwards, and the moving ship-fixed coordinate system o–xyz, where o is taken on the midship of the ship, and x, y and z axes point towards the ship's bow, towards the starboard and vertically downwards, respectively. Heading angle ψ is defined as the angle between x_0 and x axes, δ the rudder angle and r the yaw rate. u and v_m denote the velocity components in x and y directions, respectively; drift angle at midship position β is defined by $\beta = \tan^{-1}(-v_m/u)$, and the total velocity U, $U = \sqrt{u^2 + v_m^2}$. Center of gravity of the ship G is located at $(x_G, 0, 0)$ in o–xyz system. Then, lateral velocity component at the center of gravity v is expressed as

$$v = v_m + x_G r \tag{1}$$

One of the special feature of the present model is the use of the coordinate system fixed to the midship position. This may be convenient when considering the captive model tests with different load conditions like full and ballast loads. When employing the origin of the center of gravity, for instance, the coordinate of the rudder/propeller position

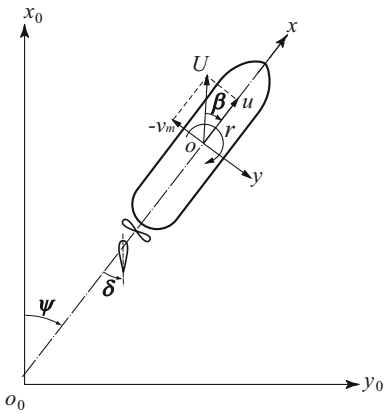

Fig. 1 Coordinate systems

changes in full and ballast load conditions since the longitudinal position of the center of gravity generally changes in different load conditions. Employing the midship-based coordinate system can avoid such the troublesome.

2.2 Motion equations

Maneuvering motions of a ship in still water are represented as surge, sway, and yaw. The motion equations are expressed as

$$\left.\begin{aligned} m(\dot{u} - vr) &= F_x \\ m(\dot{v} + ur) &= F_y \\ I_{zG}\,\dot{r} &= M_z \end{aligned}\right\} \tag{2}$$

In Eq. 2, unknown variables are u, v and r. Here, F_x, F_y and M_z are expressed as follows:

$$\left.\begin{aligned} F_x &= -m_x\dot{u} + m_y v_m r + X \\ F_y &= -m_y\dot{v}_m - m_x u r + Y \\ M_z &= -J_z\dot{r} + N_m - x_G F_y \end{aligned}\right\} \tag{3}$$

Added mass coupling terms with respect to v_m and r are neglected in view of practical purposes.

Substituting Eqs. 1 and 3 into Eq. 2 for eliminating v, the following equations are obtained:

$$\left.\begin{aligned} (m + m_x)\dot{u} - (m + m_y)v_m r - x_G m r^2 &= X \\ (m + m_y)\dot{v}_m + (m + m_x)ur + x_G m\dot{r} &= Y \\ (I_{zG} + x_G^2 m + J_z)\dot{r} + x_G m(\dot{v}_m + ur) &= N_m \end{aligned}\right\} \tag{4}$$

Eq. 4 is the motion equations to be solved.

The right-hand side of Eq. 4 X, Y and N_m is expressed as

$$\left.\begin{aligned} X &= X_{\mathrm{H}} + X_{\mathrm{R}} + X_{\mathrm{P}} \\ Y &= Y_{\mathrm{H}} + Y_{\mathrm{R}} \\ N_m &= N_{\mathrm{H}} + N_{\mathrm{R}} \end{aligned}\right\} \tag{5}$$

Subscript H, R, and P means hull, rudder, and propeller, respectively.

2.3 Hydrodynamic forces acting on ship hull

X_{H}, Y_{H} and N_{H} are expressed as follows:

$$\left.\begin{aligned} X_{\mathrm{H}} &= (1/2)\rho L_{pp} d U^2\, X'_{\mathrm{H}}(v'_m, r') \\ Y_{\mathrm{H}} &= (1/2)\rho L_{pp} d U^2\, Y'_{\mathrm{H}}(v'_m, r') \\ N_{\mathrm{H}} &= (1/2)\rho L_{pp}^2 d U^2\, N'_{\mathrm{H}}(v'_m, r'), \end{aligned}\right\} \tag{6}$$

where v'_m denotes non-dimensionalized lateral velocity defined by v_m/U, and r' non-dimensionalized yaw rate by rL_{pp}/U. X'_{H} is expressed as the sum of resistance coefficient R'_0 and the 2nd and 4th order polynomial function of v'_m and r'. Y'_{H} and N'_{H} are expressed as the 1st and 3rd order polynomial function of v'_m and r':

$$\left.\begin{aligned} X'_{\mathrm{H}}(v'_m, r') &= -R'_0 + X'_{vv}v'^2_m + X'_{vr}v'_m r' + X'_{rr}r'^2 + X'_{vvvv}v'^4_m \\ Y'_{\mathrm{H}}(v'_m, r') &= Y'_v v'_m + Y'_{\mathrm{R}}r' + Y'_{vvv}v'^3_m + Y'_{vvr}v'^2_m r' + Y'_{vrr}v'_m r'^2 + Y'_{rrr}r'^3 \\ N'_{\mathrm{H}}(v'_m, r') &= N'_v v'_m + N'_{\mathrm{R}}r' + N'_{vvv}v'^3_m + N'_{vvr}v'^2_m r' + N'_{vrr}v'_m r'^2 + N'_{rrr}r'^3, \end{aligned}\right\} \tag{7}$$

where X'_{vv}, X'_{vr}, X'_{rr}, X'_{vvvv}, Y'_v, Y'_{R}, Y'_{vvv}, Y'_{vvr}, Y'_{vrr}, Y'_{rrr}, N'_v, N'_{R}, N'_{vvv}, N'_{vvr}, N'_{vrr}, and N'_{rrr} are called the hydrodynamic derivatives on maneuvering. Note that the expression of the 1st and 3rd order polynomial function like Eq. 7 is superior to the other expression such as the 1st and 2nd order polynomial function in view of estimation accuracy for Y'_{H} and N'_{H} [3, 5].

2.4 Hydrodynamic force due to propeller

Surge force due to propeller X_{P} is expressed as

$$X_{\mathrm{P}} = (1 - t_{\mathrm{P}})T \tag{8}$$

Thrust deduction factor t_{P} is assumed to be constant at given propeller load for simplicity. Propeller thrust T is written as

$$T = \rho n_{\mathrm{P}}^2 D_{\mathrm{P}}^4 K_T(J_{\mathrm{P}}) \tag{9}$$

K_T is approximately expressed as 2nd polynomial function of propeller advanced ratio J_{P}:

$$K_T(J_{\mathrm{P}}) = k_2 J_{\mathrm{P}}^2 + k_1 J_{\mathrm{P}} + k_0 \tag{10}$$

J_{P} is written as

$$J_{\mathrm{P}} = \frac{u(1 - w_{\mathrm{P}})}{n_{\mathrm{P}} D_{\mathrm{P}}} \tag{11}$$

The w_{P} changes with maneuvering motions in general and the several formulas have been presented, for instance,

$$w_{\mathrm{P}}/w_{\mathrm{P0}} = \exp(-4\beta_{\mathrm{P}}^2) \tag{12}$$

$$(1 - w_{\mathrm{P}})/(1 - w_{\mathrm{P0}}) = 1 + C_1(\beta_{\mathrm{P}} + C_2\beta_{\mathrm{P}}|\beta_{\mathrm{P}}|)^2 \tag{13}$$

$$(1 - w_{\mathrm{P}})/(1 - w_{\mathrm{P0}}) = 1 + (1 - \cos^2\beta_{\mathrm{P}})(1 - |\beta_{\mathrm{P}}|), \tag{14}$$

where β_{P} is the geometrical inflow angle to the propeller in maneuvering motions and defined as

$$\beta_{\mathrm{P}} = \beta - x'_{\mathrm{P}} r' \tag{15}$$

Eqs. 12–14 were presented in Refs. [4, 9, 10], respectively. However, the estimation accuracy of Eqs. 12 and 14 was not enough. Also, the physical meaning of C_1 and C_2 in Eq. 13 is not clear. In this article, a formula is introduced as

$$(1 - w_{\mathrm{P}})/(1 - w_{\mathrm{P0}}) = 1 + \{1 - \exp(-C_1|\beta_{\mathrm{P}}|)\}(C_2 - 1) \tag{16}$$

From Eq. 16, we see that

$$(1 - w_{\mathrm{P}})/(1 - w_{P0}) \to C_2 \quad \text{at } |\beta_{\mathrm{P}}| \to \infty \tag{17}$$

Therefore, C_2 means value of $(1-w_P)/(1-w_{P0})$ at large $|\beta_P|$. Then, C_1 represents the wake change characteristic versus β_P. Thus, the physical meaning of C_1 and C_2 is clear for Eq. 16. The actual wake characteristic is asymmetry with respect to β_P due to the propeller rotational effect. Then, the different C_2 value should be taken for plus/minus β_P in Eq. 16. The fitting accuracy will be discussed in Sect. 4.3.

In the expression of X_P, the steering effect on the propeller thrust T is excluded. Instead of this, the effect is taken into account at the rudder force component X_R as shown in the next section.

2.5 Hydrodynamic forces by steering

Effective rudder forces X_R, Y_R and N_R are expressed as

$$\left.\begin{aligned} X_R &= -(1-t_R)F_N \sin\delta \\ Y_R &= -(1+a_H)F_N \cos\delta \\ N_R &= -(x_R + a_H x_H)F_N \cos\delta, \end{aligned}\right\} \tag{18}$$

where F_N is the rudder normal force. Note that the rudder tangential force is neglected in Eq. 18. The t_R, a_H and x_H are the coefficients representing mainly hydrodynamic interaction between ship hull and rudder. The t_R is called the steering resistance deduction factor and defined the deduction factor of rudder resistance versus $F_N \sin\delta$ which means longitudinal component of F_N [3]. Actually, X_R includes a component of the propeller thrust change due to steering as mentioned in Sect. 2.4. Therefore, t_R means a factor of both the rudder resistance deduction and the propeller thrust increase induced by steering. The propeller thrust increase occurs due to the increase of nominal wake at propeller position by steering. On the other hand, the mechanism of the rudder resistance deduction by steering is not clear at present, although the rudder tangential force component neglected in Eq. 19 may involve t_R.

The a_H and x_H are called the rudder force increase factor and the position of an additional lateral force component, respectively. The a_H represents the factor of lateral force acting on ship hull by steering versus $F_N \cos\delta$ which means the lateral component of F_N. The magnitude of a_H was almost 0.3–0.4 in tank tests [9], and this means that the lateral force acting on the ship by steering increases about 30–40 % larger than the rudder normal force component. The x_H means the longitudinal acting point of the additional lateral force component. The measured value of x_H was almost $-0.45L_{pp}$ and the additional force acts on the stern part of the hull. This phenomena may be understandable when considering the hydrodynamic interaction of a wing with a flap. Then, ship hull and rudder are regarded as the main wing and the flap, respectively, as shown in Fig. 2. Lift force is induced on the rudder itself by steering, and at the same time, an additional force component, ΔY in Fig. 2, is induced on the ship hull. The ΔY comes from the hydrodynamic interaction between hull (main wing) and rudder (flap). Then, a_H is defined by $-\Delta Y/F_N \cos\delta$, and x_H can be regarded as the acting point of ΔY. This phenomena was pointed by Karasuno [11] and theoretically confirmed by Hess [12].

Rudder normal force F_N is expressed as

$$F_N = (1/2)\rho A_R U_R^2 f_\alpha \sin\alpha_R \tag{19}$$

Here, the resultant rudder inflow velocity U_R and the angle α_R are expressed as

$$U_R = \sqrt{u_R^2 + v_R^2} \tag{20}$$

$$\alpha_R = \delta - \tan^{-1}\left(\frac{v_R}{u_R}\right) \simeq \delta - \frac{v_R}{u_R} \tag{21}$$

Assuming that the helm angle is zero when β and r' are zero, v_R can be expressed as follows:

$$v_R = U\gamma_R \beta_{R0} \tag{22}$$

Here, γ_R is called the flow straightening coefficient and usually smaller than 1.0. This means that the actual inflow angle to rudder becomes smaller than the geometrical inflow angle β_{R0}. The flow straightening phenomena comes from the presence of hull and propeller slip stream as shown in Fig. 3. The β_{R0} is expressed as the sum of hull drift angle β and inflow velocity change due to yaw motion $-x'_R r'$. Here, x'_R is non-dimensional longitudinal coordinate of rudder position and should be -0.5. However, obtaining the value of x'_R in the experiments actually, it was not -0.5 and close to -1.0 [9]. This means that the flow straightening phenomena in turning motion is not so simple. Here, the effective inflow angle to rudder β_R is newly defined using a new symbol ℓ'_R instead of x'_R. Then, v_R is expressed as

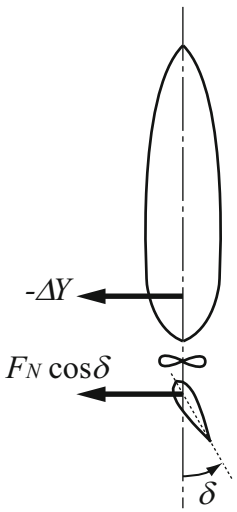

Fig. 2 Schematic figure of rudder force and the additional lateral force induced by steering

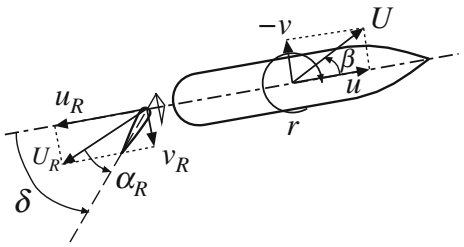

Fig. 3 Rudder inflow velocity and angle

$$v_{\mathrm{R}} = U\,\gamma_{\mathrm{R}}\beta_{\mathrm{R}} \tag{23}$$

where

$$\beta_{\mathrm{R}} = \beta - \ell'_{\mathrm{R}} r' \tag{24}$$

Here, ℓ'_{R} is treated as an experimental constant for expressing v_{R} accurately and can be obtained from the captive model test.

The γ_{R} characteristic considerably affects the maneuvering simulation, so we have to capture it correctly. Value of γ_{R} generally takes different magnitude for port and starboard turning and this is one of the reasons for asymmetrical turning motions in port and starboard. The flow straightening effect was pointed out by Fujii and Tuda [13] first, and after that a form of Eq. 23 was proposed by Kose et al. [9].

A longitudinal inflow velocity component to rudder u_{R} is expressed referring to the derivation described in Appendix as follows:

$$u_{\mathrm{R}} = \varepsilon\, u(1-w_{\mathrm{P}})\sqrt{\eta\left\{1+\kappa\left(\sqrt{1+\frac{8K_T}{\pi J_{\mathrm{P}}^2}}-1\right)\right\}^2+(1-\eta)}, \tag{25}$$

where ε means a ratio of wake fraction at rudder position to that at propeller position defined by $\varepsilon = (1-w_{\mathrm{R}})/(1-w_{\mathrm{P}})$. The κ is an experimental constant.

3 Captive model test and the results

In this section, outline of captive model tests is described to capture the hydrodynamic force characteristics. As an example, the experimental data opened in SIMMAN2008 workshop [6] for KVLCC2 model is introduced.

3.1 A sample ship: KVLCC2

A VLCC tanker called KVLCC2 [7] was selected as a sample ship. Table 1 shows the principal particulars. In the table, the principal particulars of ship models with 2.909 m length (L3-model) and with 7.00 m length(L7-model) are shown together with those of fullscale ship. L3-model was used for the captive model tests conducted at National Maritime Research Institute, Japan, to capture the hydrodynamic force characteristics [6]. L7-model was used for the free-running model tests conducted in a square tank of MARIN[8]. The body plan is shown in Fig. 4. This ship has a mariner rudder. Note that A_{R} in Table 1 is a profile area of movable part of the rudder excluding the horn part.

Table 1 Principal particulars of a KVLCC2 tanker

	L3-model	L7-model	Fullscale
Scale	1/110	1/45.7	1.00
L_{pp} (m)	2.902	7.00	320.0
B (m)	0.527	1.27	58.0
d (m)	0.189	0.46	20.8
∇ (m^3)	0.235	3.27	312,600
x_G (m)	0.102	0.25	11.2
C_b	0.810	0.810	0.810
D_{P} (m)	0.090	0.216	9.86
H_{R} (m)	0.144	0.345	15.80
A_{R} (m^2)	0.00928	0.0539	112.5

3.2 Outline of captive model tests

3.2.1 Kind of tests

The captive tests were carried out at propelled condition of a ship model with a rudder model. Ship speed U_0 was set at 0.76 m/s (equivalent to 15.5 kn in fullscale). As the propeller loading point the model point was selected in principle.

In advance of the captive model tests, resistance test, self-propulsion test, and propeller open water test were carried out. After that, the following tests were conducted:

1. Rudder force test in straight moving under various propeller loads.
2. Oblique towing test (OTT) and circular motion test (CMT).
3. Rudder force test in oblique towing and steady turning conditions (flow straightening coefficient test).

Rudder force test in straight moving is the test to measure the hydrodynamic forces acting on the ship model when the ship moves straight with keeping a certain rudder angle. From this test, the hull rudder interaction coefficients (t_{R}, a_{H}, x'_{H}) and the parameters for representing the longitudinal inflow velocity component to rudder (κ, ε) can be obtained.

OTT and CMT are the test to measure the hydrodynamic forces acting on the ship model in oblique moving and/or steady turning. Then, the rudder angle should be

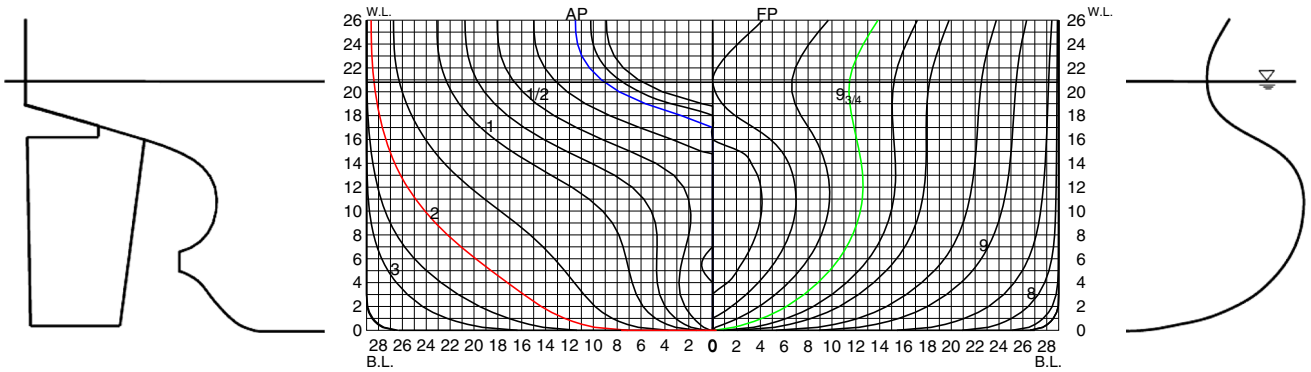

Fig. 4 Body plan and profiles of KVLCC2 tanker

zero. From the tests, the hydrodynamic forces acting on the ship and the wake fractions at propeller position in maneuvering motions can be obtained. Planar motion technique (PMM) test is widely used as a method to capture the hydrodynamic derivatives on turning. The hydrodynamic derivatives obtained by PMM test remarkably change due to influence of the motion frequency and the motion amplitude given in the test and it is difficult to select the proper values for the maneuvering simulations. To avoid the uncertainty, CMT was employed here instead of PMM test.

The flow straightening coefficient test is the test to capture the rudder angle where the normal force becomes zero (δ_{FN0}) and the inclination of the normal force coefficient versus rudder angle at δ_{FN0} in oblique moving and/or steady turning ($dF'_N/d\delta$). The flow straightening coefficient (γ_R) is determined from the results of δ_{FN0} and $dF'_N/d\delta$.

All the tests were carried out in the free condition for trim and sinkage of the model.

3.2.2 Measurement items

Measurement items in the tests are as follows:

- Surge force, lateral force and yaw moment around midship acting on the ship model (X, Y, N_m),
- rudder normal force (F_N),
- propeller thrust (T).

3.3 Test results

3.3.1 Rudder force test results in straight moving

Figure 5 shows the rudder force test results in straight moving under various propeller loads. In the test, the rudder angle was changed in the range of $-20°$ to $20°$ or $-35°$ to $35°$ with $5°$ interval at several different propeller load conditions. Then, propeller revolution n_P was changed as 14.48, 17.95, and 24.87 rps with keeping U_0 constant so as to cover the range of both ship point and model point. Absolute values of the hydrodynamic force coefficients Y', N'_m and F'_N increase with increase of the propeller revolution n_P and/or the rudder angle δ.

3.3.2 OTT and CMT results

Hull drift angle β was changed in the range of $-20°$ to $20°$ in OTT, and non-dimensional yaw rate r' was changed in the range of -0.8–0.8 with 0.2 interval with a certain drift angle in CMT. The range of β and r' in the tests was determined so as to cover the actual maneuvering motions. Figure 6 shows OTT and CMT results: X'_{mes}, Y'_{mes}, N'_{mes}, F'_N and T' versus β and r'. Here, X'_{mes}, Y'_{mes}, and N'_{mes} are the actual measured forces in which the inertia forces such as the centrifugal force acting on the turning ship are included.

3.3.3 Flow straightening coefficient test results

Direct measurements of δ_{FN0} and $dF'_N/d\delta$ are difficult in oblique moving and/or steady turning. These were captured by the following procedure:

1. Rudder normal forces are measured with changing 3 rudder angles. These 3 rudder angles have to be selected appropriately so as the rudder angle at zero normal force can be determined.
2. δ_{FN0} is determined by an interpolation based on 3 measured rudder normal force results versus δ.
3. $dF'_N/d\delta$ is numerically calculated by taking an inclination of the rudder normal force coefficient versus δ.

Figure 7 shows δ_{FN0} and $dF'_N/d\delta$ as functions of β and r'. The δ_{FN0} increases with increasing β or r'; however, $dF'_N/d\delta$ does not change very much with β or r'.

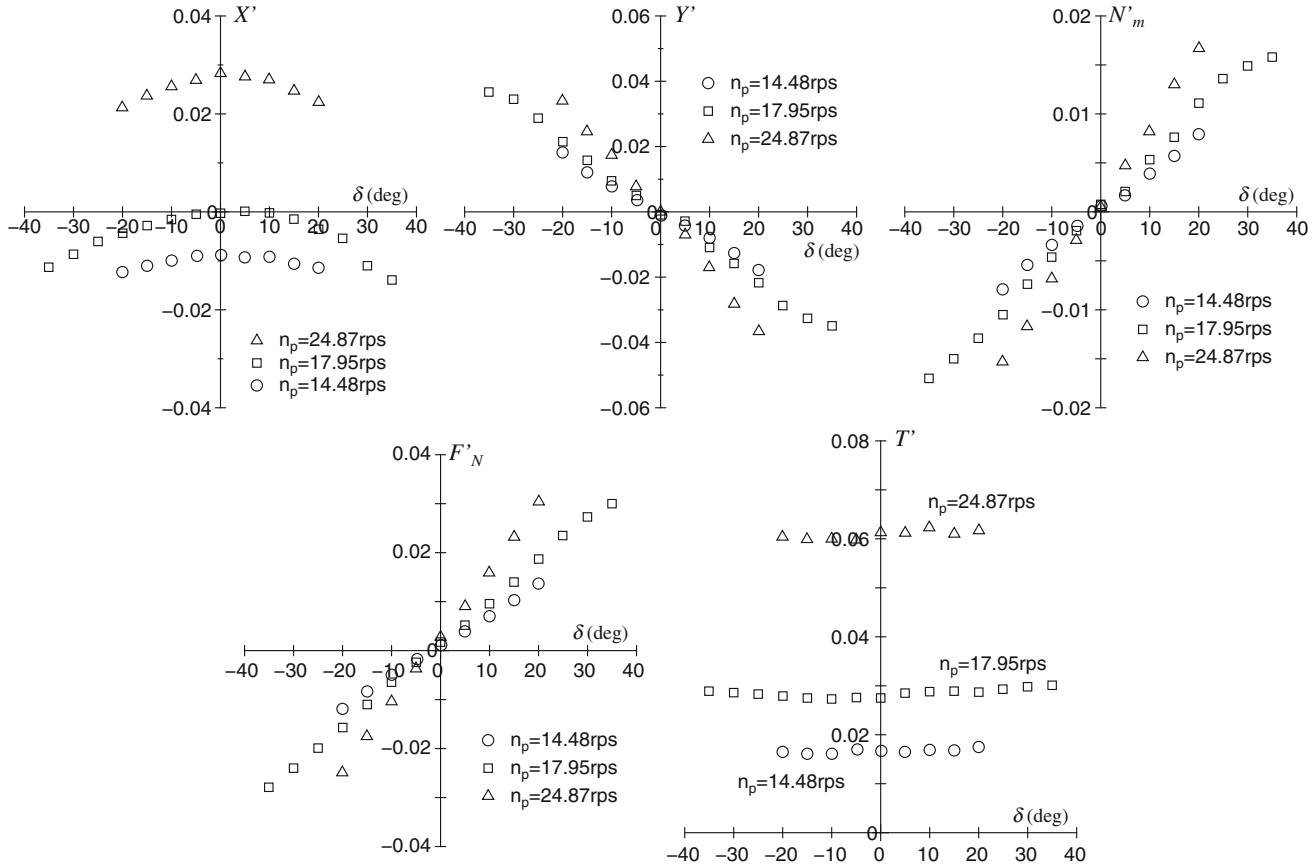

Fig. 5 Rudder force test results in straight moving under various propeller loads for KVLCC2 model

4 Determination of hydrodynamic force coefficients

Next, analysis methods are described to determine the hydrodynamic force coefficients defined in the simulation model referring to Ref. [5].

4.1 t_R, a_H and x'_H

The rudder force tests in straight moving are conducted in the condition of $\beta = r' = 0$, so that Y_H and N_H should be zero in Eq. 5. Then, the non-dimensional forms of eq.(5) are written as follows:

$$\left.\begin{aligned} X' &= -R'_0 + (1-t_P)T' - (1-t_R)F'_N \sin\delta \\ Y' &= -(1+a_H)F'_N \cos\delta \\ N'_m &= -(x'_R + a_H x'_H)F'_N \cos\delta \end{aligned}\right\} \quad (26)$$

From Eq. 26, we know the following:

- $(1-t_R)$ is determined as an inclination of X' versus $-F'_N \sin\delta$. Note that R'_0 and $(1-t_P)T'$ are not related to the rudder angle δ in the simulation model.
- $(1+a_H)$ is determined as an inclination of Y' versus $-F'_N \cos\delta$.
- $(x'_R + a_H x'_H)$ is determined as an inclination of N'_m versus $-F'_N \cos\delta$. Then, x'_H can be calculated since x'_R is -0.5 and a_H is known.

It is experimentally confirmed that the inclinations of X', Y' and N'_m can be approximated as a linear function. Namely, t_R, a_H and x'_H can be regarded as constant values at given propeller load. The hull rudder interaction coefficients are usually determined at a representative propeller load (in this case, $n_P = 17.95$ rps, model point), although there is a trend that a_H slightly decreases with increase of propeller load[14].

Figure 8 shows the figures used for determining the hull rudder interaction coefficients. From the figures, it was determined that t_R, a_H and x'_H are 0.387, 0.312, and -0.464, respectively.

4.2 Hydrodynamic derivatives on maneuvering

The hydrodynamic derivatives on maneuvering are determined from OTT and CMT results. The inertia force components are included to the hydrodynamic forces measured in CMT. Then, the actual measured force coefficients (X'_{mes}, Y'_{mes}, N'_{mes}) are theoretically expressed as follows:

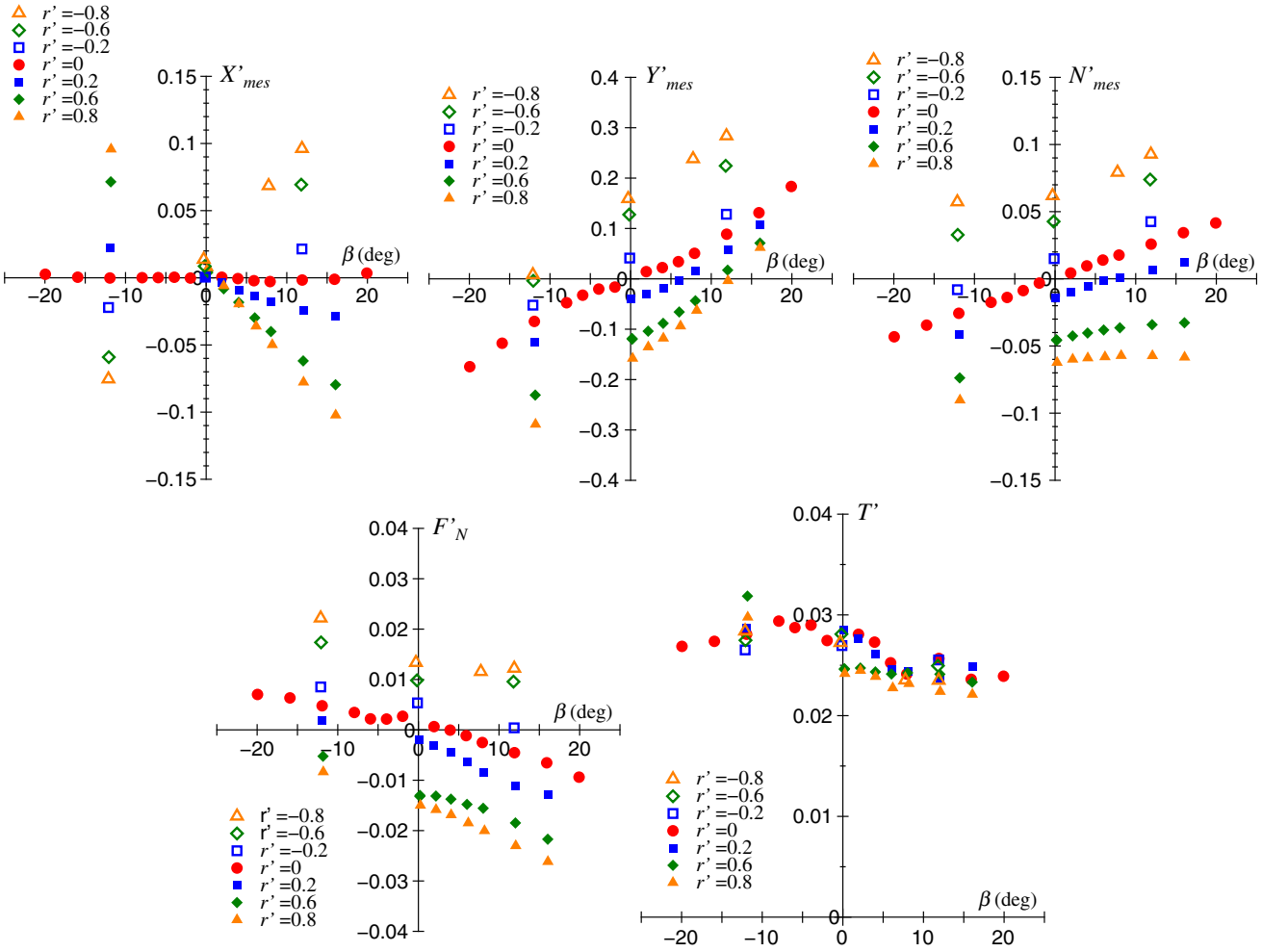

Fig. 6 OTT and CMT results for KVLCC2 model

$$\left.\begin{aligned} X'_{\mathrm{mes}} &= X'^{*}_{\mathrm{H}} + X'_{\mathrm{R}} + X'_{\mathrm{P}} \\ Y'_{\mathrm{mes}} &= Y'^{*}_{\mathrm{H}} + Y'_{\mathrm{R}} \\ N'_{\mathrm{mes}} &= N'^{*}_{\mathrm{H}} + N'_{\mathrm{R}} \end{aligned}\right\} \tag{27}$$

where

$$\left.\begin{aligned} X'^{*}_{\mathrm{H}} &= X'_{\mathrm{H}} + (m' + m'_y)v'_m r' + x'_G m' r'^2 \\ Y'^{*}_{\mathrm{H}} &= Y'_{\mathrm{H}} - (m' + m'_x)r' \\ N'^{*}_{\mathrm{H}} &= N'_{\mathrm{H}} - x'_G m' r' \end{aligned}\right\} \tag{28}$$

Here, an approximation of $u' \simeq 1$ was employed. In Eq. 28, $(m' + m'_y)v'_m r'$, $-(m' + m'_x)r'$, etc. are inertia force terms including added mass components. Considering the situation in CMT, namely taking $\delta = 0$ in Eq. 27, the following equations are obtained:

$$\left.\begin{aligned} X'^{*}_{\mathrm{H}} &= X'_{\mathrm{mes}} - (1 - t_{\mathrm{P}})T' \\ Y'^{*}_{\mathrm{H}} &= Y'_{\mathrm{mes}} + (1 + a_{\mathrm{H}})F'_N \\ N'^{*}_{\mathrm{H}} &= N'_{\mathrm{mes}} + (x'_{\mathrm{R}} + a_{\mathrm{H}} x'_{\mathrm{H}})F'_N \end{aligned}\right\} \tag{29}$$

Using Eq. 29, X'^{*}_{H}, Y'^{*}_{H} and N'^{*}_{H} can be calculated since X'_{mes}, Y'_{mes}, N'_{mes}, F'_N, and T' are measured, and t_{P}, t_{R}, a_{H}, and x'_{H} are given. On the other hand, substituting Eq. 7 to Eq. 28, X'^{*}_{H}, Y'^{*}_{H}, and N'^{*}_{H} are written as a function of v'_m and r' as follows:

$$\left.\begin{aligned} X'^{*}_{\mathrm{H}} &= -R'_0 + X'_{vv}v'^2_m + (X'_{vr} + m' + m'_y)v'_m r' + (X'_{rr} + x'_G m')r'^2 + X'_{vvvv}v'^4_m \\ Y'^{*}_{\mathrm{H}} &= Y'_v v'_m + (Y'_{\mathrm{R}} - m' - m'_x)r' + Y'_{vvv}v'^3_m + Y'_{vvr}v'^2_m r' + Y'_{vrr}v'_m r'^2 + Y'_{rrr}r'^3 \\ N'^{*}_{\mathrm{H}} &= N'_v v'_m + (N'_{\mathrm{R}} - x'_G m')r' + N'_{vvv}v'^3_m + N'_{vvr}v'^2_m r' + N'_{vrr}v'_m r'^2 + N'_{rrr}r'^3 \end{aligned}\right\} \tag{30}$$

Each term in Eq. 30 such as Y'_v, $(Y'_{\mathrm{R}} - m' - m'_x)$, N'_v, $(N'_{\mathrm{R}} - x'_G m')$, etc. is determined by a least square method (LSM) based on calculated X'^{*}_{H}, Y'^{*}_{H} and N'^{*}_{H} using Eq. 29. In terms of $(X'_{vr} + m' + m'_y)$, $(X'_{rr} + x'_G m')$, $(Y'_{\mathrm{R}} - m' - m'_x)$, and $(N'_{\mathrm{R}} - x'_G m')$, mass and added mass components are included. Then, m' is given from the displacement volume of the ship, but m'_x and m'_y are unknown. The added mass components have to be estimated by other method.

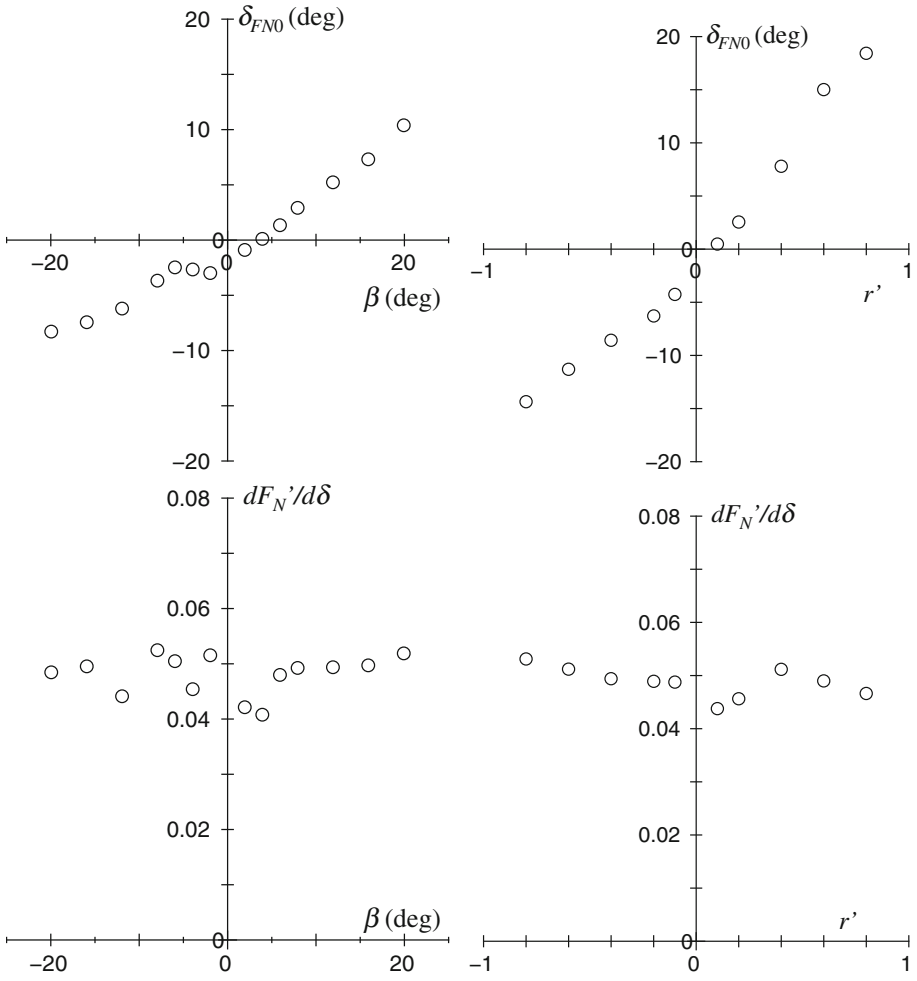

Fig. 7 δ_{FN0} and $dF'_N/d\delta$ obtained in flow straightening coefficient test for KVLCC2 model

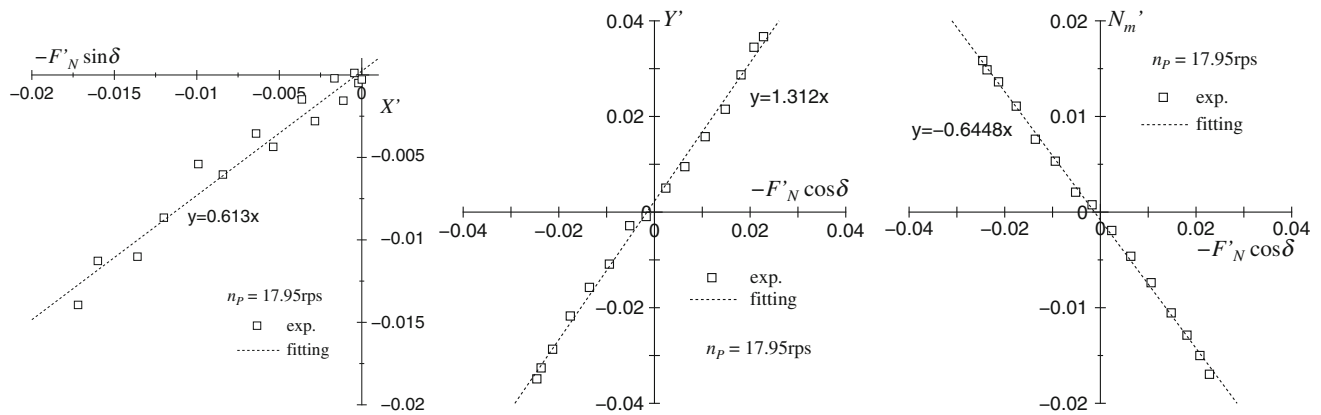

Fig. 8 Analysis results for hull and rudder interaction coefficients of KVLCC2 model

Figure 9 shows obtained $X_{\mathrm{H}}^{*'}$, $Y_{\mathrm{H}}^{*'}$ and $N_{\mathrm{H}}^{*'}$. The hydrodynamic derivatives obtained by LSM are listed in Table 2. To confirm the accuracy of expression of Eq. 30, the fitting curves expressed as dotted line are also plotted in Fig. 9. The fitting accuracy is sufficient in view of practical purposes.

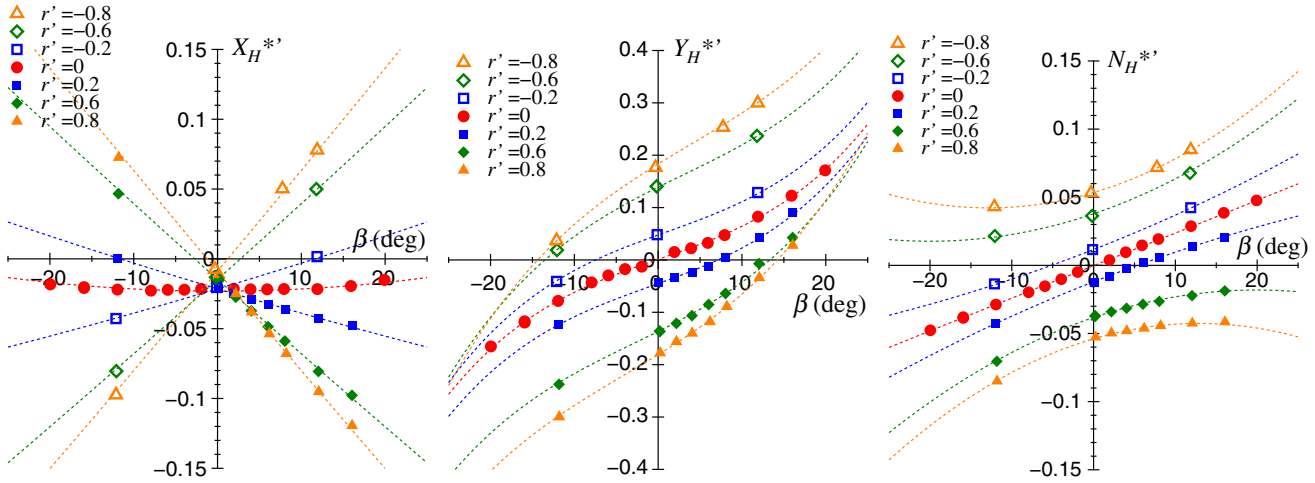

Fig. 9 Analysis results of hydrodynamic forces acting on KVLCC2 model @

Table 2 Resistance coefficient and hydrodynamic derivatives on maneuvering

R'_0	0.022	Y'_v	−0.315	N'_v	−0.137
X'_{vv}	−0.040	$Y'_R - m' - m'_x$	−0.233	$N'_R - x'_G m'$	−0.059
$X'_{vr} + m' + m'_y$	0.518	Y'_{vvv}	−1.607	N'_{vvv}	−0.030
$X'_{rr} + x'_G m'$	0.021	Y'_{vvr}	0.379	N'_{vvr}	−0.294
X'_{vvvv}	0.771	Y'_{vrr}	−0.391	N'_{vrr}	0.055
		Y'_{rrr}	0.008	N'_{rrr}	−0.013

4.3 w_P

Wake coefficient in maneuvering motions w_P is obtained by the thrust identification method using the propeller open water characteristic based on the propeller thrust measured in OTT and CMT. Figure 10 shows the obtained wake fraction as the function of β_P. As shown in Fig. 10, the wake characteristic is asymmetry with respect to the horizontal axis β_P. The fitting line is also plotted using Eq. 16 with $C_2 = 1.6$ at $\beta_P > 0$ and $C_2 = 1.1$ at $\beta_P < 0$. Equation 16 has practically enough accuracy.

4.4 γ_R and ℓ'_R

The γ_R and ℓ'_R are determined from the measured results of δ_{FN0} and $dF'_N/d\delta$. Basic formulas are derived for analysis of γ_R and ℓ'_R here. Non-dimensionalizing Eq. by combining Eqs. 20 and 21, the following formula is obtained:

$$F'_N = \frac{A_R}{L_{pp}d}(u'^2_R + v'^2_R) f_\alpha \sin\left(\delta - v'_R/u'_R\right) \tag{31}$$

Differentiating Eq. 31 by δ is obtained as

$$\frac{dF'_N}{d\delta} = \frac{A_R}{L_{pp}d}(u'^2_R + v'^2_R) f_\alpha \cos\left(\delta - v'_R/u'_R\right) \tag{32}$$

Then, Eq. 32 is rewritten using a relation of $\delta_{FN0} = v'_R/u'_R$ as

$$\left.\frac{dF'_N}{d\delta}\right|_{\delta=\delta_{FN0}} = \frac{A_R}{L_{pp}d} u'^2_R (1 + \delta^2_{FN0}) f_\alpha \tag{33}$$

From Eq. 33, the following formula is obtained:

$$u'_R = \sqrt{\left.\frac{dF'_N}{d\delta}\right|_{\delta=\delta_{FN0}} \frac{L_{pp}d}{A_R} \frac{1}{f_\alpha(1 + \delta^2_{FN0})}} \tag{34}$$

The u'_R can be calculated by Eq. 34 since δ_{FN0} and $dF'_N/d\delta$ at $\delta = \delta_{FN0}$ are experimentally given.

The v'_R can be calculated using a relation of $v'_R = u'_R \delta_{FN0}$. On the other hand, v'_R is expressed from Eq. 23 as

$$v'_R = \gamma_R(\beta - \ell'_R r') \tag{35}$$

The γ_R is determined based on the v'_R calculated in oblique towing condition as an inclination of the fitting line. After that, ℓ'_R is determined in the same manner.

Figure 11 shows the analysis result of rudder inflow velocity v'_R. The v'_R characteristic is obviously different in plus and minus of β_R. From the figure, $\gamma_R = 0.395$ at $\beta_R < 0$ and $\gamma_R = 0.640$ at $\beta_R > 0$ were obtained.

4.5 κ and ε

The ε and κ can be determined from the rudder force test results in straight moving under various propeller loads.

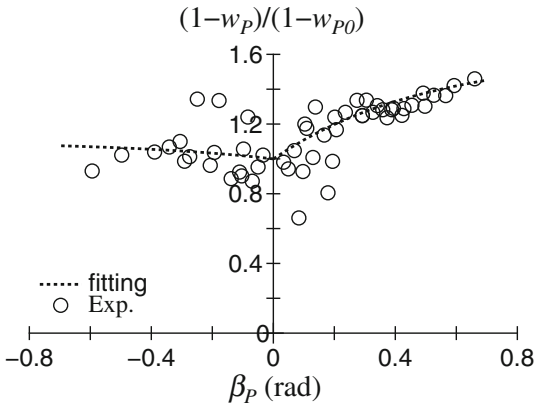

Fig. 10 Analysis results of wake fraction in maneuvering motions for KVLCC2 model

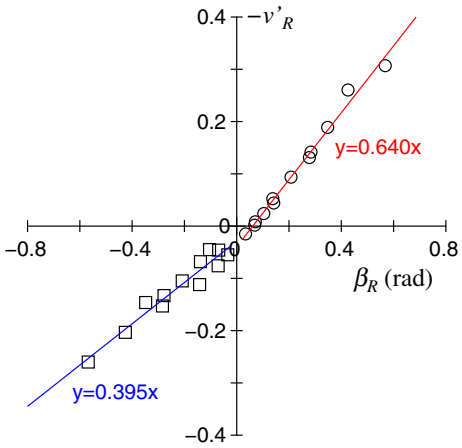

Fig. 11 Analysis result of rudder inflow velocity v'_R for KVLCC2 model

Substituting $v'_R = 0$ into Eq. 32, the following formula is obtained:

$$\left.\frac{dF'_N}{d\delta}\right|_{\delta=0} = \frac{A_R}{L_{pp}d}\, u'^2_R\, f_\alpha \tag{36}$$

The u'^2_R can be obtained from Eq. 36 since $dF'_N/d\delta|_{\delta=0}$ and f_α are known. On the other hand, u'^2_R is expressed from Eq. 25 as

$$u'^2_R = \varepsilon^2 (1-w_P)^2 \eta \left\{ 1 + \kappa \left(\sqrt{1 + \frac{8K_T}{\pi J_P^2}} - 1 \right) \right\}^2 + (1-\eta) \tag{37}$$

The result of u'^2_R calculated using Eq. 37 has to coincide with the result of u'^2_R obtained using Eq. 36. The ε and κ are determined so as to minimize the difference between the two u'^2_R. Then, the iterative procedure is needed to obtain ε and κ.

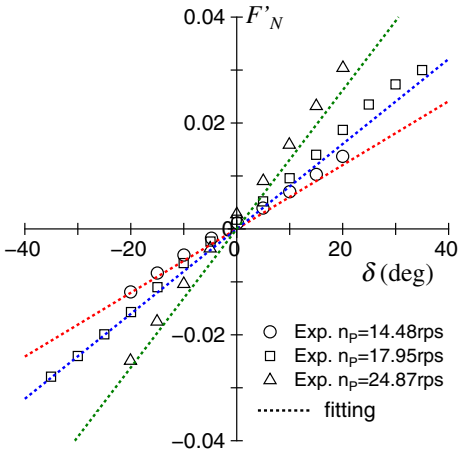

Fig. 12 Analysis results of rudder normal force in different propeller load conditions for KVLCC2 model

Figure 12 shows F'_N versus δ measured in the test and the fitting result using Eq. 37. As a result of the analysis, $\varepsilon = 1.09$ and $\kappa = 0.50$ were obtained. The fitting accuracy is sufficient in view of practical purposes, although some discrepancy between fitting line and experiments is observed due to existing of small helm angle in the experiments.

5 Maneuvering simulations

5.1 Details of simulations

Simulations are made for turning with $\delta = \pm 35°$, and 10/10 and 20/20 zig-zag maneuvers. Table 3 shows the hydrodynamic force coefficients used in the simulations. Other parameters and treatments for the simulations are as follows:

- Hull resistance was calculated by a 3-dimensional extrapolation method based on Schoenherr's frictional resistance coefficient formula.
- Parameters of propeller thrust open water characteristic were as follows: $(k_0, k_1, k_2) = (0.2931, -0.2753, -0.1385)$.
- Effective wake in straight moving w_{P0} was assumed to be 0.40 for L7-model and 0.35 for fullscale.
- Added mass coefficients (m'_x, m'_y, J'_z) listed in Table 3 were estimated by Motora's empirical charts [16–18].
- Rudder lift gradient coefficient f_α was estimated using Fujii's formula expressed as [13]:

$$f_\alpha = \frac{6.13\Lambda}{\Lambda + 2.25} \tag{38}$$

Table 3 Hydrodynamic force coefficients used in the simulations

X'_{vv}	−0.040	m'_x	0.022
X'_{vr}	0.002	m'_y	0.223
X'_{rr}	0.011	J'_z	0.011
X'_{vvvv}	0.771	t_P	0.220
Y'_v	−0.315	t_R	0.387
Y'_R	0.083	a_H	0.312
Y'_{vvv}	−1.607	x'_H	−0.464
Y'_{vvr}	0.379	C_1	2.0
Y'_{vrr}	−0.391	C_2 $(\beta_P > 0)$	1.6
Y'_{rrr}	0.008	C_2 $(\beta_P < 0)$	1.1
N'_v	−0.137	γ_R $(\beta_R < 0)$	0.395
N'_R	−0.049	γ_R $(\beta_R > 0)$	0.640
N'_{vvv}	−0.030	ℓ'_R	−0.710
N'_{vvr}	−0.294	ε	1.09
N'_{vrr}	0.055	κ	0.50
N'_{rrr}	−0.013	f_α	2.747

This formula can be regarded as a modified version of Prandtl's formula based on the lifting line theory. Here, Λ is aspect ratio of a rudder including the horn part. Hirano et al. [15] proposed a practical treatment when applying Eq. 38 to Mariner rudder: a whole rudder with the horn part is used for determining f_α and a movable part area is used as a representative rudder area. Values of f_α and A_R were determined by this treatment.

- In the simulations, we set that an initial approach speed U_0 is 15.5 kn in fullscale, the rudder steering rate is $1.76\,^\circ/s$ in fullscale, and the radius of yaw gyration is $0.25L_{pp}$. Propeller revolution is assumed to be kept the revolution at U_0 constant without torque rich.

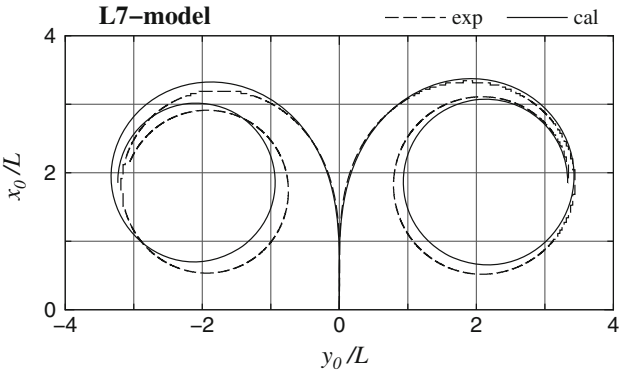

Fig. 13 Comparison of ship trajectories (L7-model, $\delta = \pm 35°$)

Table 4 Comparison of turning indices

	Cal.	Exp.
A'_D $(\delta = 35°)$	3.31	3.25
D'_T $(\delta = 35°)$	3.36	3.34
A'_D $(\delta = -35°)$	3.26	3.11
D'_T $(\delta = -35°)$	3.26	3.08

5.2 Comparison with free-running model test results

First, maneuvering simulations were made for L7-model of KVLCC2. Figure 13 shows comparison of calculation and experiment in turning trajectories with $\delta = \pm 35°$. Table 4 shows comparison of turning indices such as A'_D and D'_T. The turning simulation results roughly agree with the free-running model test results, although the turning indices calculated are about 5.8 % larger in maximum than the test results.

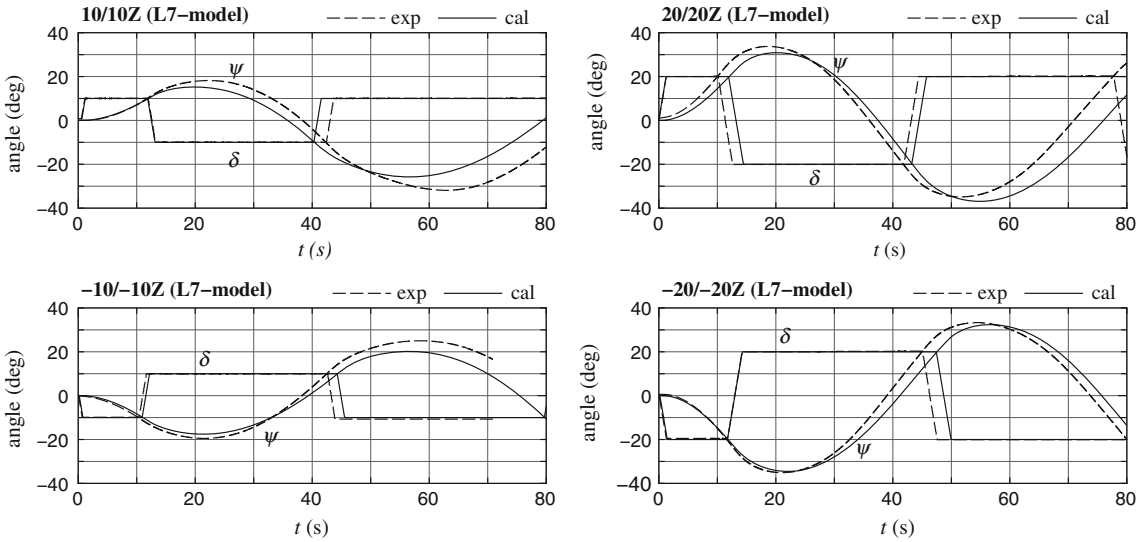

Fig. 14 Comparison of time histories of rudder angle and heading angle in zig-zag maneuvers (L7-model)

Table 5 Comparison of overshoot angles of zig-zag maneuvers (L7-model)

	Cal. (°)	Exp. (°)
1st OSA (10/10Z)	5.2	8.2
2nd OSA (10/10Z)	15.8	21.9
1st OSA (20/20Z)	10.9	13.7
1st OSA (−10/−10Z)	7.6	9.5
2nd OSA (−10/−10Z)	10.2	15.0
1st OSA (−20/−20Z)	14.5	15.1

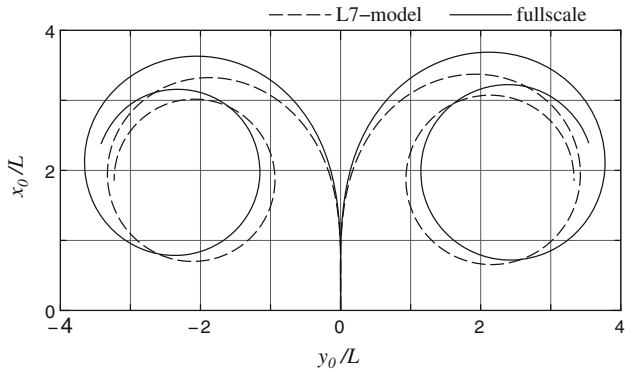

Fig. 15 Simulation results of turning trajectories for L7-model and fullscale ($\delta = \pm 35°$)

Figure 14 shows comparisons of calculation and experiment for time histories of rudder angle (δ) and heading angle (ψ) in zig-zag maneuvers. The simulation results roughly agree with the free-running model test results, and the present method can capture the overall tendency of the zig-zag maneuvers. Table 5 shows comparison of overshoot angles (OSAs) in the zig-zag maneuvers. Maximum differences of OSA between calculation and experiment are about 3° for 1st OSA and about 6° for 2nd OSA of 10/10 zig-zag maneuver. It is difficult to predict OSA in the accuracy of a few degrees. All the OSAs calculated by the present method are smaller than the test results. There is a possibility that hull damping force used in the simulations is a bit too larger than actual one.

5.3 Simulation results in fullscale

Next, maneuvering simulations were made for fullscale ship of KVLCC2 tanker. In the simulations, the same hydrodynamic force coefficients used in the simulations of the ship model were used except the effective wake in straight moving w_{P0} and the frictional resistance coefficient calculated by Schoenherr's formula. Figure 15 shows simulation results of turning trajectories with $\delta = \pm 35°$ for L7-model and fullscale, and Table 6 the turning indices. Fullscale turning trajectories becomes look like expanding outside as shown in Fig. 15, and A'_D and D'_T in fullscale are about 10 % larger comparing with L7-model. This means that turning performance becomes worse in fullscale.

Table 6 Simulation results of turning indices

	L7-model	fullscale
A'_D ($\delta = 35°$)	3.31	3.62
D'_T ($\delta = 35°$)	3.36	3.71
A'_D ($\delta = -35°$)	3.26	3.56
D'_T ($\delta = -35°$)	3.26	3.59

Figure 16 shows time histories of δ and ψ for L7-model and fullscale in zig-zag maneuvers. In Fig. 16, the horizontal axis means non-dimensionalized time defined as $t' \equiv tU_0/L_{pp}$. Table 7 shows overshoot angles for L7-model and fullscale. In fullscale, overshoot angle becomes large, timing of steering for zig-zag maneuver is slow, and yaw response against steering becomes worse. Thus, the course stability becomes worse in fullscale.

To know the reason for a change for the worse of not only turning performance but also course stability, time histories of the rudder normal force during turning with $\delta = 35°$ were compared in fullscale and model. Figure 17 shows the time histories of non-dimensionalized rudder normal force (F'_N) divided by $(1/2)\rho L_{pp} d U_0^2$. Peak value of F'_N in fullscale is about 20% smaller than that of the ship model. This is a main cause for bad maneuverability in fullscale. At the steady turning stage, F'_N in fullscale is about 40 % smaller than that of the model and the difference becomes large. Propeller load is relatively smaller in fullscale so that the rudder inflow velocity also becomes small. As a result, the rudder normal force becomes small in fullscale.

6 Concluding remarks

In this article, a prototype of maneuvering prediction method for ships, called "MMG standard method", was introduced. The MMG standard method was composed of 4 elements: the maneuvering simulation model, the procedure of the required captive model tests to capture the hydrodynamic force characteristics, the analysis method for determining the hydrodynamic force coefficients for maneuvering simulations, and the prediction method for maneuvering motions in fullscale. KVLCC2 tanker was selected as a sample ship and the captive mode test results were presented with a process of the data analysis. Using the hydrodynamic force coefficients obtained, maneuvering simulations were carried out for KVLCC2 model [8] and the fullscale ship for validation of the method. It was confirmed that the present method can roughly capture the

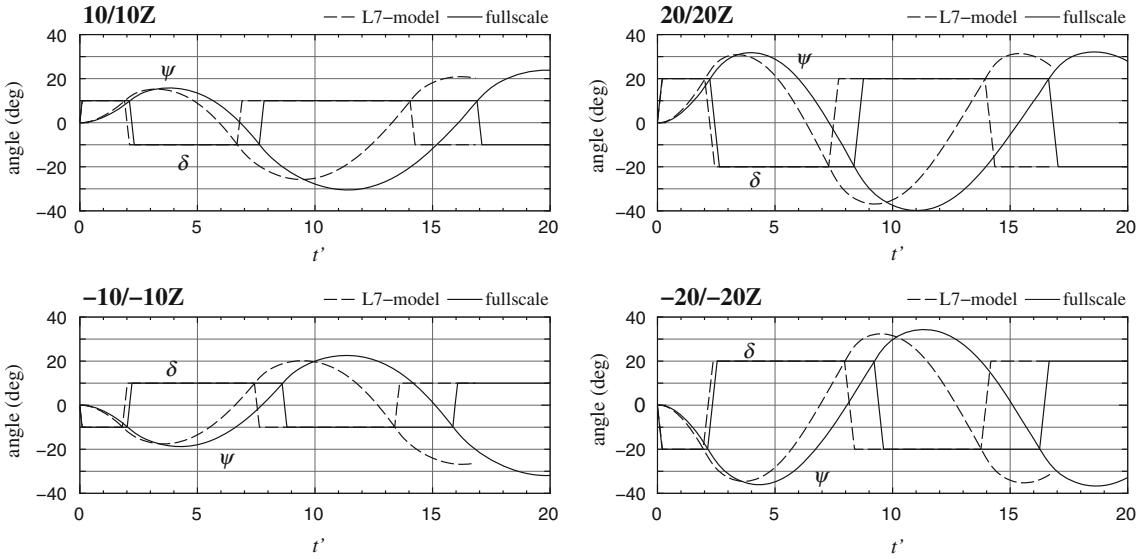

Fig. 16 Simulation results of time histories of rudder angle and heading angle in zig-zag maneuvers for L7-model and fullscale

Table 7 Simulation results of overshoot angles of zig-zag maneuvers

	L7-mode (°)	Fullscale (°)
1st OSA (10/10Z)	5.2	5.8
2nd OSA (10/10Z)	15.8	20.5
1st OSA (20/20Z)	10.9	11.8
1st OSA (−10/−10Z)	7.6	8.8
2nd OSA (−10/−10Z)	10.2	12.6
1st OSA (−20/−20Z)	14.5	16.1

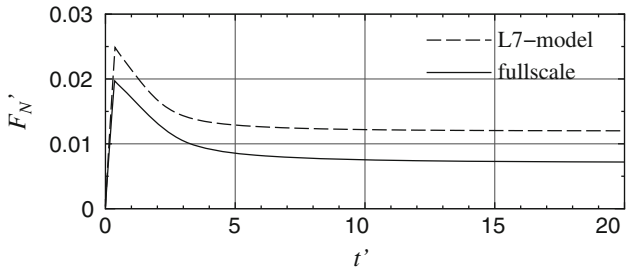

Fig. 17 Time histories of rudder normal force during turning for L7-model and fullscale ($\delta = 35°$)

maneuvering motions and is useful for the maneuvering predictions in fullscale.

Collecting the hydrodynamic force coefficients determined by the MMG standard method in various ship kinds is the next work to make a useful data base of the force coefficients for ship maneuvering predictions.

Acknowledgments We would like to express our thanks to committee members of "Research committee on standardization of mathematical model for ship maneuvering predictions" organized by the Japan Society of Naval Architects and Ocean Engineers. The experimental data analysis presented in this article was carried out by Mr. S. Ito as a part of his master course study. We would like to extend our thanks to him.

Appendix A: Derivation of a formula representing inflow velocity component to rudder

Consider the longitudinal velocity component to rudder u_R according to Ref. [9]. The u_R is assumed to be expressed as

$$u_R = \sqrt{\frac{A_{RP}}{A_R}u_{RP}^2 + \frac{A_{R0}}{A_R}u_{R0}^2} = \sqrt{\eta u_{RP}^2 + (1-\eta)u_{R0}^2}, \quad (39)$$

where A_{RP} is the rudder area where propeller slip stream hits, A_{R0} the rudder area where it does not hit, and A_R the total rudder area (namely, $A_R = A_{R0} + A_{RP}$). Equation 39 is obtained to take a weighted average of 2 velocity components, u_{RP} at A_{RP} and u_{R0} at A_{R0}, as shown in Fig. 18. Here, η is expressed as

$$\eta = \frac{A_{RP}}{A_R} \simeq \frac{D_P}{H_R} \quad (40)$$

The η can be calculated taking a ratio between propeller diameter D_P and rudder span length H_R.

The u_{R0} is expressed by introducing w_R which is wake coefficient at A_{R0} as

$$u_{R0} = (1 - w_R)u \quad (41)$$

Also, u_{RP} is assumed to be expressed as

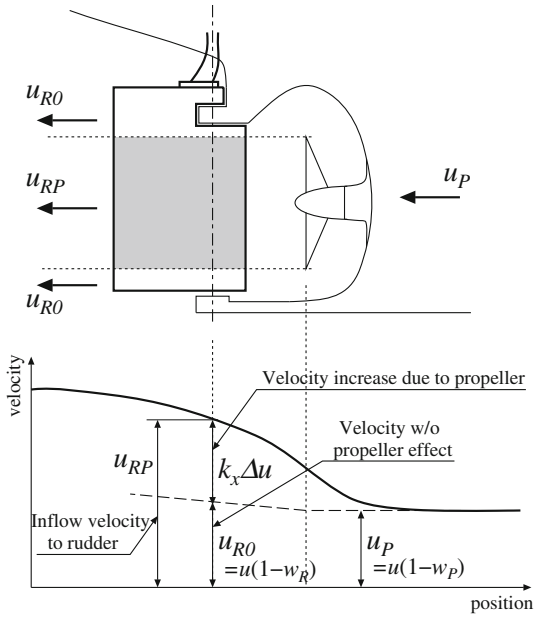

Fig. 18 A diagram of inflow velocity to rudder behind the propeller

$$u_{\mathrm{RP}} = u_{\mathrm{R0}} + k_x \Delta u \tag{42}$$

Here, $k_x\Delta u$ means the velocity increase due to influence of propeller slip stream, where Δu is the theoretical velocity increase described later and k_x the correction factor, and is expressed as $\Delta u = u_\infty - u_{\mathrm{P}}$ where u_∞ is the velocity at infinite rear position, and u_{P} the propeller inflow velocity which is expressed as $u_{\mathrm{P}} = (1 - w_{\mathrm{P}})u$. There exists a relation between u_∞ and u_{P} from Bernoulli's theorem as

$$\Delta p + \frac{\rho}{2} u_{\mathrm{P}}^2 = \frac{\rho}{2} u_\infty^2, \tag{43}$$

where Δp denotes a pressure difference between fore and aft at propeller disc. T is expressed using Δp:

$$T = \Delta p \, \pi \left(\frac{D_{\mathrm{P}}}{2} \right)^2 \tag{44}$$

In addition, taking expression of Eq. 9, u_∞ is written as

$$u_\infty = u_{\mathrm{P}} \sqrt{1 + \frac{8K_T}{\pi J_{\mathrm{P}}^2}} \tag{45}$$

Substituting Eqs. 41, 42, and 45 to Eq. 39 for eliminating Δu and u_∞, the following formula is obtained as

$$u_{\mathrm{R}} = \varepsilon u_{\mathrm{P}} \sqrt{\eta \left\{ 1 + \kappa \left(\sqrt{1 + \frac{8K_T}{\pi J_{\mathrm{P}}^2}} - 1 \right) \right\}^2 + (1 - \eta)}, \tag{46}$$

where ε is defined by $\varepsilon = (1 - w_{\mathrm{R}})/(1 - w_{\mathrm{P}})$, and κ is a constant defined by k_x/ε.

References

1. Ogawa A, Koyama T, Kijima K (1977) MMG report-I, on the mathematical model of ship manoeuvring. Bull Soc Naval Archit Jpn 575:22–28 (in Japanese)
2. Ogawa A, Kasai H (1978) On the mathematical method of manoeuvring motion of ships. Int Shipbuild Prog 25(292):306–319
3. Matsumoto K, Suemitsu K (1980) The prediction of manoeuvring performances by captive model tests. J Kansai Soc Naval Archit Jpn 176:11–22 (in Japanese)
4. Inoue S, Hirano M, Kijima K, Takashina J (1981) A practical calculation method of ship maneuvering motion. Int Shipbuild Prog 28(325):207–222
5. (2013) Report of Research committee on standardization of mathematical model for ship maneuvering predictions (P-29), Japan Society of Naval Architects and Ocean Engineers (in Japanese). http://www.jasnaoe.or.jp/research/p_committee_end.html
6. Yoshimura Y, Ueno M, Tsukada Y (2008) Analysis of steady hydrodynamic force components and prediction of manoeuvring ship motion with KVLCC1, KVLCC2 and KCS, SIMMAN 2008, Workshop on verification and validation of ship manoeuvring simulation method, Workshop Proceedings, vol 1, Copenhagen, pp E80–E86
7. (2008) SIMMAN 2008: part B benchmark test cases, KVLCC2 description. Workshop on verification and validation of ship manoeuvring simulation method, Workshop Proceedings, vol 1, Copenhagen, pp B7–B10
8. (2008) SIMMAN 2008: part C captive and free model test data. Workshop on verification and validation of ship manoeuvring simulation method, Workshop Proceedings, vol 1, Copenhagen
9. Kose K, Yumuro A, Yoshimura Y (1981) III. Concrete of mathematical model for ship manoeuvring. In: Proceedings of the 3rd symposium on ship maneuverability, Society of Naval Architects of Japan, pp 27–80 (in Japanese)
10. Yoshimura Y (1986) Mathematical model for the manoeuvring ship motion in shallow water. J Kansai Soc Naval Archit Jpn 200:41–51 (in Japanese)
11. Karasuno K (1969) Studies on the lateral force on a hull induced by rudder deflection. J Kansai Soc Naval Archit Jpn 133:14–19 (in Japanese)
12. Hess F (1978) Lifting-surface theory applied to ship-rudder systems. Int Shipbuild Prog 25(292):299–305
13. Fujii H, Tuda T (1961) Experimental research on rudder performance (2). J Soc Naval Archit Jpn 110:31–42 (in Japanese)
14. Yasukawa H (1992) Hydrodynamic interactions among hull, rudder and propeller of a turning thin ship. Trans West-Jpn Soc Naval Archit 84:59–83
15. Hirano M, Takashina J, Moriya S, Fukushima M (1982) Open water performance of semi-balanced rudder. Trans West-Jpn Soc Naval Archit 64:93–101
16. Motora S (1959) On the measurement of added mass and added moment of inertia for ship motions. J Soc Naval Archit Jpn 105:83–92 (in Japanese)
17. Motora S (1960) On the measurement of added mass and added moment of inertia for ship motions (part 2. Added mass for the longitudinal motions). J Soc Naval Archit of Jpn 106:59–62
18. Motora S (1960) On the measurement of added mass and added moment of inertia for ship motions (part 3. Added mass for the transverse motions). J Soc Naval Archit Jpn 106:63–68 (in Japanese)